Applied Energy 346 (2023) 121390

Contents lists available at ScienceDirect

Applied Energy

journal homepage: www.elsevier.com/locate/apenergy

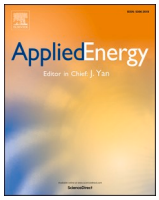

Model predictive control of a microgrid with energy-stored quasi-Z-source cascaded H-bridge multilevel inverter and PV systems

Pablo Horrillo-Quintero [a], Pablo García-Triviño [a], Raúl Sarrias-Mena [b], Carlos A. García-Vázquez [a], Luis M. Fernández-Ramírez [a,*]

[a] Research Group in Sustainable and Renewable Electrical Technologies (PAIDI-TEP023), Department of Electrical Engineering, Higher Technical School of Engineering of Algeciras (ETSIA), University of Cádiz, Avda. Ramón Puyol, s/n. 11202 Algeciras (Cádiz), Spain

[b] Research Group in Sustainable and Renewable Electrical Technologies (PAIDI-TEP023), Department of Engineering in Automation, Electronics and Computer Architecture & Networks, Higher Technical School of Engineering of Algeciras (ETSIA), University of Cádiz, Avda. Ramón Puyol, s/n. 11202 Algeciras (Cádiz), Spain

HIGHLIGHTS

- Study of microgrid with energy-stored quasi-Z-source cascaded H-bridge multilevel inverter and PV system.
- Development of energy management system based on model predictive control (MPC-EMS).
- Results compared with proportional sharing algorithm based on SOC level (SOC-EMS).
- Best results obtained from MPC-EMS.

ARTICLE INFO

Keywords:
Microgrid
Photovoltaic power plant
Battery energy storage system
Quasi-Z-source cascaded H-bridge multilevel inverter
Energy management system
Model predictive control

ABSTRACT

This paper presents a new energy management system (EMS) based on model predictive control (MPC) for a microgrid with solar photovoltaic (PV) power plants and a quasi-Z-source cascaded H-bridge multilevel inverter that integrates an energy storage system (ES-qZS-CHBMLI). The system comprises three modules, each with a PV power plant, quasi-impedance network, battery energy storage system (BESS), and voltage source inverter (VSI). Traditional EMS methods focus on distributing the power among the BESSs to balance their state of charge (SOC), operating in charging or discharging mode. The proposed MPC-EMS carries out a multi-objective control for an ES-qZS-CHBMLI topology, which allows an optimized BESS power distribution while meeting the system operator requirements. It prioritizes the charge of the BESS with the lowest SOC and the discharge of the BESS with the highest SOC. Thus, both modes can coexist simultaneously, while ensuring decoupled power control. The MPC-EMS proposed herein is compared with a proportional sharing algorithm based on SOC (SOC-EMS) that pursues the same objectives. The simulation results show an improvement in the control of the power delivered to the grid. The Integral Time Absolute Error, ITAE, achieved with the MPC-EMS for the active and reactive power is 20 % and 4 %, respectively, lower than that obtained with the SOC-EMS. A 1,3 % higher charge for the BESS with the lowest SOC is also registered. Furthermore, an experimental setup based on an OPAL RT-4510 unit and a dSPACE MicroLabBox prototyping unit is implemented to validate the simulation results.

1. Introduction

The impact of global warming, as a consequence of the constant increase in energy demand in cities and industries [1], promotes the development of microgrids (MGs) as an improvement to the traditional electric power systems. The MG concept was developed to integrate distributed energy resources (DERs) and energy storage systems (ESSs) in a controlled and safe way[2,3]. In this context, a MG can be defined as a group of distributed loads and energy sources, with clearly defined electrical boundaries, that acts as a single and controllable entity [4]. Furthermore, it can operate either connected to grid or islanded.

Among the different renewable electrical technologies (RETs),

* Corresponding author.
E-mail addresses: pablo.horrillo@uca.es (P. Horrillo-Quintero), pablo.garcia@uca.es (P. García-Triviño), raul.sarrias@uca.es (R. Sarrias-Mena), carlosandres.garcia@uca.es (C.A. García-Vázquez), luis.fernandez@uca.es (L.M. Fernández-Ramírez).

https://doi.org/10.1016/j.apenergy.2023.121390
Received 26 April 2023; Accepted 31 May 2023
Available online 12 June 2023

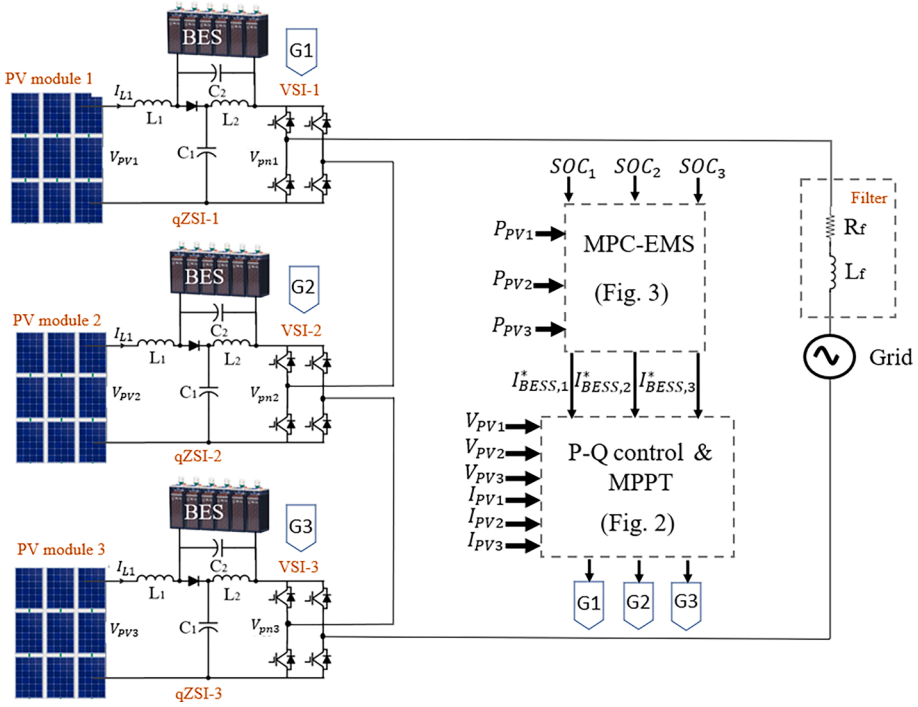

Fig. 1. Configuration of the MG under study.

photovoltaic (PV) generation covers a relevant portion of the energy generation mix in many countries [5]. Power conversion in typical PV power plants is carried out in two stages using DC/DC and DC/AC converters [6]. Recently, the use of impedance source inverters (ZSI) and quasi-impedance source inverters (qZSI) has gained interest owing to their advantages. For instance, DC/AC conversion can be performed in a single stage, and a higher voltage boost is achieved when compared with the traditional voltage-source inverter (VSI) [7,8]. Despite these advantages, there are high-power applications where the voltage gap between the PV system and the utility grid is excessively high for a single qZSI [9]. In such circumstances, several qZSI modules can be interconnected to build a qZS-cascaded H-bridge multilevel inverter (qZS-CHBMLI). The principle of operation of the cascaded configuration has been defined in literature [10]. In addition, qZS-CHBMLI has interesting properties, such as low total harmonic distortion (THD), decreased switching power losses, and higher fault tolerance [11].

However, the main problem associated with PV generation is its stochastic nature [12]. To solve this problem, ESSs are usually implemented to support PV power generation by smoothing out variations in the power generation. One of the most widely used energy storage technologies in MGs are Lithium-Ion batteries [13], because of their high efficiency and long lifetime.

The combination of RETs and ESSs requires a control system to coordinate the power exchange. This control system is typically referred to as the energy management system (EMS). In [14], an EMS was implemented to balance the power of a battery energy storage system (BESS) between two safe state of charge (SOC) limits in an energy storage quasi-impedance cascaded H-bridge multilevel inverter (ES-qZS-CHBMLI). Ref. [15] presented an improvement of the aforementioned EMS to increase the lifetime of the BESS, making all the BESSs work as a single unit during charge and discharge. The EMS architecture proposed in [16] combines the BESS balancing system based on SOC levels and the DC bus voltage regulation system into a single system. A SOC-based adaptive droop control method was proposed in [17], in order to balance the SOC of several BESSs in MG applications. Recently, new EMS algorithms, such as fuzzy logic, neural networks, genetic algorithms and model predictive control (MPC) have gained interest [18]. Ref. [19] presented a review of the applications of fuzzy logic in renewable energy systems. This review indicated that fuzzy-based models provide realistic estimates for power point tracking and optimization in power distribution. The authors in [20] implemented an online biogeography-based optimization (BBO) algorithm as the EMS of a hybrid system integrating a BESS, qZSI and PV generator connected to the grid. The BBO algorithm improved the BESS current control and required less computation time compared with the particle swarm optimization (PSO) algorithm. The MPC proposed in [21] was based on a multi-objective cooperative control combining maximum power point tracking (MPPT), battery power and point of common coupling (PCC) current management for a single qZSI with PV and BESS system. In this regard, MPC was suitable for handling multi-objective coordinated control tasks. The MPC-EMS presented in [22] consisted of an effective and stable dynamic power management system (PMS) for a MG combining batteries, fuel cells and supercapacitors as ESSs. In [23], an optimal MPC-based EMS designed for long-term studies was analysed. This system was composed of a PV generator, BESS, and hydrogen production. This EMS allowed reducing the operating cost of the microgrid. The authors in [24] suggested an MPC-EMS for a hybrid energy storage system consisting of an electrolyzer, a fuel cell, and a battery. The MPC acted as the central controller located in the second level of its hierarchical control. On the other hand, a MPC was implemented in [25] in a DC MG with PV generation, BESS and a DC load. This EMS allowed the PV system to operate at the maximum power point (MPP), and to regulate the common DC bus voltage using the BESS. Two different MPCs were presented in [26] for an AC MG with a PV system and BESS. The first MPC was responsible for voltage control in islanded mode, and the other one managed the power in grid-connected mode. In [27], a MPC-based system without any proportional-integrative-derivative (PID) controller was presented for a MG with PV generation, wind turbine and BESS. A first MPC was in charge of controlling the DC/DC converter, and a second one managed the DC/AC converter. The permanent magnet synchronous generator (PMSGs)-based DC MG proposed in [28] was founded on a distributed MPC, where the upper layer controllers coordinated the operation of grid-side converters, thus providing power references for each PMSG. Ref. [29] proposed the application of a

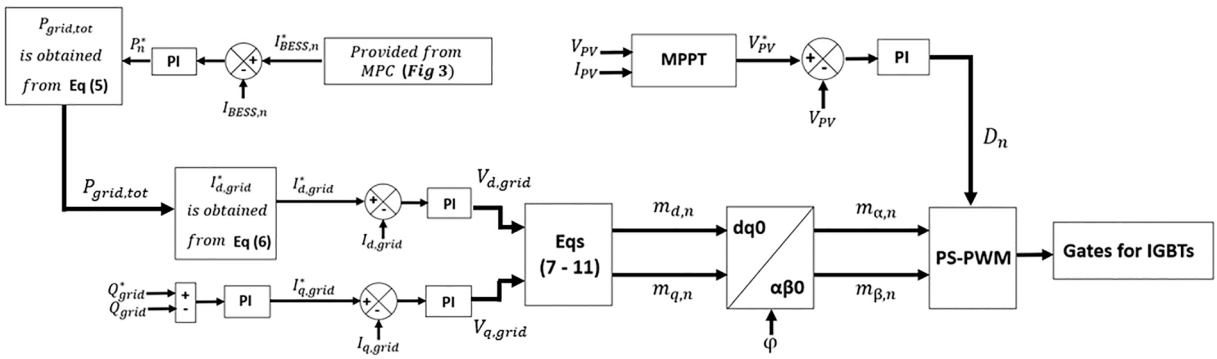

Fig. 2. Control scheme for the ES-qZS-CHBMLI.

finite control set model predictive control (FCS-MPC) strategy in standalone AC MGs. The authors in [30] analysed the application of MPC to the economic power dispatch of a hybrid ESS. In [31], the MPC for DC/DC converters in PV-based MGs developed an advanced control technique for voltage regulation and stabilization of converters. A decentralized power management system based on MPC for an AC MG was presented in [32]. The AC MG consisted of DC/DC converter, DC/AC converter, PV generator and BESS. The bidirectional BESS converter maintained the DC bus voltage and the SOC balance of the BESS. The hierarchical control developed in [33] demonstrated that MPC can be used to implement a control scheme with both primary and secondary levels for an islanded AC MG. A configuration with a single qZSI and PV system was implemented in [34]. It was based on MPC to achieve decoupled control of active and reactive powers.

Few studies have addressed the dynamics of AC MGs with PV power plants, ESS and MPC-EMS connected to the utility grid. In most works, a DC/DC converter was used to implement the MPPT strategy for PV power plants [27–32], and a VSI was commonly used for DC/AC conversion[33,34], The topology proposed herein is based on ES-qZS-CHBMLI, without additional DC/DC converters, allowing a single-stage power conversion. Furthermore, this configuration ensures independent MPPT operation for each PV system. The control system implemented allows a decoupled control of active and reactive powers. In addition, the BESSs can support PV generators, storing or supplying energy according to the setpoints of the EMS. The main contribution of this work is the implementation of a MPC-based EMS for an ES-qZS-CHBMLI in an AC MG with PV power plants and BESS. The proposed EMS allows to control the SOC levels and the total power of the BESS. The MPC has four inputs (SOC of each BESS, and total BESSs power) and three outputs (current reference for each BESS). The MPC-EMS performs an efficient power distribution among the BESSs. This implies that the BESS with the lowest SOC can be charged, whereas other BESSs operate in discharging mode. In addition, the BESS with the highest SOC will provide more power than the other BESSs. Regarding the control scheme, a direct control of the active power delivered to the grid is used instead of an indirect control through PV generation and BESSs power. In addition, this EMS guarantees a decoupled control of the active and reactive power injected to the grid for an ES-qZS-CHBMLI configuration.

The remainder of this article is organized as follows: Section 2 describes the configuration of the proposed system. Section 3 details the design of the control system. Section 4 describes the proposed MPC-EMS. Section 5 presents a SOC-EMS used to compare the proposed MPC-EMS. The results obtained from the simulation and the experimental setup are presented and discussed in Section 6. Finally, the main conclusions of this work are presented in Section 7.

2. Configuration of the system

The MG under study consists of three modules in series connected to a single-phase utility grid. Each module is composed of a PV generator, an impedance network with a BESS and a single-phase VSI. This modular configuration allows the independent MPPT control of the PV generators and simultaneous management of the active and reactive power delivered to the grid. The configuration of the system is shown in Fig. 1.

The Lithium-Ion batteries connected in parallel with the capacitors $C_{2,n}$ (where n is the number of modules connected in series) in the impedance networks are the BESSs selected to smooth the fluctuations of the PV generators. A quasi-impedance network is implemented to boost the PV voltage, instead of the traditional DC/DC converter. In addition to removing DC/DC converters from the system, the use of qZSI brings other advantages. Mainly, a lower voltage stress in the capacitors $C_{2,n}$, no need for additional filtering capacitors, and a reduced switching ripple.

The operating principle of qZSI has been described in the literature [35]. According to [36], the voltage of the DC link, i.e. the DC voltage at the input of the VSI ($V_{pn,n}$), and the currents through the inductors 1 and 2 ($I_{L1,n}, I_{L2,n}$) in steady state are given by:

$$V_{pn,n} = \frac{V_{C1,n}}{1 - D_n} \tag{1}$$

$$I_{L1,n} = I_{L2,n} = \frac{P_{PV,n}}{V_{PV},n} \tag{2}$$

where $V_{C1,n}$ is the voltage across the capacitor $C_{1,n}$ of the impedance network, D_n is the shoot-through (ST) duty ratio of module n, which is a dimensionless parameter that relates the switching cycle (T) and the duration of the ST state (TST), $P_{PV,n}$ is the power supplied by the PV module, and $V_{PV,n}$ is the PV output voltage.

3. Control system

The control system proposed in this paper performs two different functions: 1) it implements a MPPT strategy for each PV generator; and 2) it tracks the active (P) and reactive (Q) power references set by the system operator for the MG. The MPPT and the grid power control can be achieved through two independent variables, the shoot-through duty ratio (D_n), and the modulation index (M_n), as described in subsections 3.1 and 3.2.

3.1. Maximum power point tracking

Firstly, D_n is used to regulate the PV voltage (V_{PVn}) of each module according to the reference set by the MPPT algorithm, and to boost the PV voltage. Perturb & Observe (P&O) is the MPPT algorithm responsible for obtaining the PV reference voltage (V_{PVn}^*) at each moment. P&O uses V_{PVn} and the PV current (I_{PVn}) as inputs to the algorithm, and outputs V_{PVn}^*. A PI controller adjusts D_n to track the reference V_{PVn}^*, as represented in Fig. 2. This scheme allows to maximize the PV power generation in the MG for different irradiation and temperature conditions. In this work, the algorithm is updated every 80 ms.

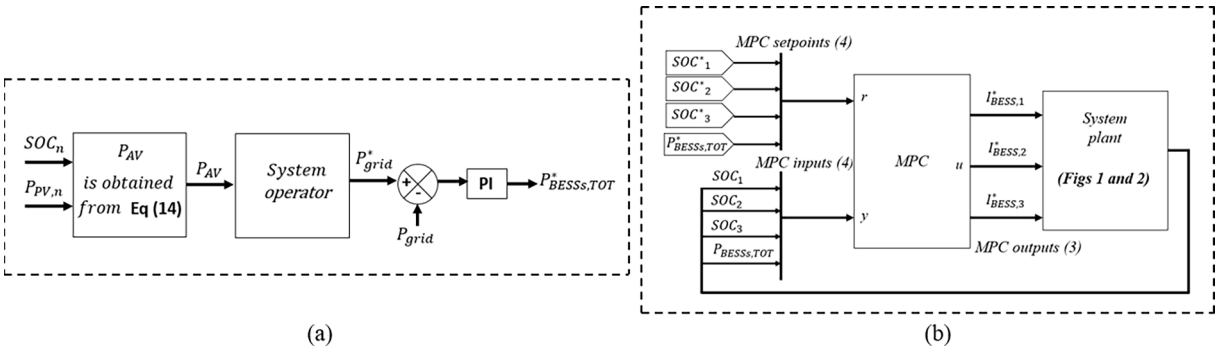

Fig. 3. MPC-EMS overall scheme: (a) Grid power control scheme. (b) MPC structure.

3.2. Power grid control

As it can be seen in Fig. 2, the control scheme for the power delivered to the grid is implemented in the direct and quadrature (d-q) reference frame for a single-phase system. Its main objective is to address the power requirements of the grid effectively. Two independent current control loops, one for P and the other for Q, are used in this case. To achieve this objective, the power control is designed as follows:

First, the single-phase grid voltage and current are measured and expressed in an orthogonal stationary reference frame with a real (α) and an imaginary (β) component.

$$V_\alpha = V_{grid} \bullet \sin(wt + \varphi) \tag{3}$$

$$V_\beta = V_{grid} \bullet \sin\left(wt + \varphi - \frac{\pi}{2}\right) \tag{4}$$

Then, the orthogonal stationary αβ frame is transformed to a rotational d-q reference frame. A phase locked loop (PLL) is employed to obtain the phase angle of the grid voltage used for synchronization in the d-q frame. Thus, the direct and quadrature components of the grid voltage ($V_{d,grid}$, $V_{q,grid}$) and current ($I_{d,grid}$, $I_{q,grid}$) are calculated to implement a decoupled control scheme based on PI controllers.

The total power to be injected into the grid is calculated as the sum of the power of each qZSI module in series:

$$P_{grid,tot} = \sum P_n^* \tag{5}$$

where P_n^* denotes the power at the DC input of each VSI. P_n^* is obtained from a PI controller, which adjusts the current of each battery $(I_{BESS,n})$ according to the reference current obtained by the EMS $\left(I_{BESS,n}^*\right)$, as illustrated in Fig. 2. The peak value of the direct current delivered to the grid ($I_{d,grid}^*$) is given by (6). This current is the same for each module because of the series connection.

$$I_{d,grid}^* = \frac{2\hat{A}\cdot P_{grid,tot}}{V_{d,grid}} \tag{6}$$

where $V_{d,grid}$ is the d component of the grid voltage. Then, $V_{d,grid}$ can be adjusted by a PI controller, which tracks $I_{d,grid}$ to its reference ($I_{d,grid}^*$). The modulation technique used in this work is the phase-shift PWM (PS-PWM), and thus, the direct component of the modulation index for each module ($m_{d,n}$) can be calculated as follows:

$$m_{d,n} = \frac{2 \bullet a_{n,P} \bullet V_{d,grid}}{V_{pn,n}} \tag{7}$$

$$a_{n,P} = \frac{P_n^*}{P_{\text{grid},tot}} \tag{8}$$

where $a_{n,P}$ is an index that denotes the active power contribution of each module with respect to the total active power delivered to the grid. $V_{pn,n}$ can be calculated by (1).

A current control loop is also used for Q. In this case, a PI controller adjusts the reference for the quadrature component of the grid current ($I_{q,grid}^*$) to track the reactive power to its reference (Q^*). The quadrature component of the grid voltage ($V_{q,grid}$) is obtained as the output of a PI controller that adjusts $I_{q,grid}$ to track $I_{q,grid}^*$. Then, the quadrature component of the modulation index for each module ($m_{q,n}$) can be expressed as follows:

$$m_{q,n} = \frac{2 \bullet a_{n,Q} \bullet V_{q,grid}}{V_{pn,n}} \tag{9}$$

$$a_{n,Q} = \frac{Q_n^*}{Q_{\text{grid},tot}} \tag{10}$$

$$Q_{grid,tot} = \sum Q_n^* \tag{11}$$

where $a_{n,Q}$ is an index that denotes the reactive power contribution of each module with respect to the total reactive power exchanged with the grid, and $Q_{\text{grid},tot}$ is the total reactive power calculated as the sum of the reactive power of each qZSI module in series (Q_n^*).

The dq components of the modulation index (m_d and m_q) are transformed into αβ components using the phase angle of the grid voltage. The real component of the modulation index ($m_{\alpha,n}$) and the shoot-through duty ratio (D_n) are used in the PS-PWM modulation technique based on Simple Boost Control (SBC) to obtain the switching signals for the IGBTs of the ES-qZS-CHBMLI. According to [35–37], SBC employs two reference signals lines for the upper and lower envelope of the modulating waves. The upper (V_p) and lower (V_n) references are defined by (12)-(13).

$$V_p = 1 - D \tag{12}$$

$$V_n = D - 1 \tag{13}$$

The maximum shoot-through duty ratio $D_{n,max}$ is $1 - M_n$. The duration of the shoot-through state is constant in each switching cycle, and therefore, the boost factor (B) is also constant.

4. Model predictive Control-Based energy management system (MPC-EMS)

In PV power plants based on multilevel inverters, the power delivered by each bridge can fluctuate owing to non-uniform solar irradiation. In most studies, the EMSs for CHBMLI configurations focus on balancing the SOC of the BESSs, considering that the BESSs act as a single unit. In such configurations, even though multiple combinations of power from the BESSs can meet the power requirements defined by the system operator, the optimal combination, in terms of control effectiveness, cannot be reached. This paper presents a new EMS based on MPC for multi-objective control targets. Its main objective is to satisfy the active and reactive power setpoints defined by the system operator

Table 1
MPC parameters.

Item	Parameter	Value
Controller parameters	T_s Sample time (s)	0.005
	P_H Prediction horizon (s)	17
	C_H Control horizon (s)	3
Constraints MV	$I_{BESS,1}$ BESS 1 current (A)	[−43.63, 43.63]
	$I_{BESS,2}$ BESS 2 current (A)	[−43.63, 43.63]
	$I_{BESS,3}$ BESS 3 current (A)	[−43.63, 43.63]
Constraints MV	SOC_1 BESS 1 SOC (%)	[15, 90]
	SOC_2 BESS 2 SOC (%)	[15, 90]
	SOC_3 BESS 3 SOC (%)	[15, 90]
	$P_{BESSs,TOT}$ Total BESSs Power (W)	[−3600, 3600]
Weights MO	SOC_1 BESS 1 SOC (%)	0.1
	SOC_2 BESS 2 SOC (%)	0.1
	SOC_3 BESS 3 SOC (%)	0.1
	$P_{BESSs,TOT}$ Total BESSs Power (W)	500
Equal Constraints Relaxation (ECR)	SOC_1 BESS 1 SOC (%)	0.01
	SOC_2 BESS 2 SOC (%)	0.01
	SOC_3 BESS 3 SOC (%)	0.01
	$P_{BESSs,TOT}$ Total BESSs Power (W)	0.5

with an optimal power distribution among the BESSs according to their SOC, as well as to maintain the SOC levels between two safe operating values. The proposed MPC-EMS computes an optimal power distribution under different operating conditions, such as changes in the power setpoints imposed by the system operator and in the PV generation. Therefore, each BESS will be charged or discharged depending on its SOC, coexisting both operation modes for different BESSs at the same time. In the existing literature, the EMSs typically perform a SOC balancing strategy and thus, all the BESSs operate in the same regime.

In this work, a detailed description of the MPC-EMS applied to an ES-qZS-CHBMLI is provided. The structure, based on four inputs (BESSs SOC levels and total BESS power) and three outputs (BESSs current references), allows an optimized tracking of the active and reactive powers delivered to the grid. Furthermore, the constraints included in the MPC design lead to a power distribution based on SOC levels. The constraints are defined to keep the BESSs operating between a high SOC (SOC_{high}) and a low SOC (SOC_{low}). In addition, the maximum BESS power is limited to their rated power (P^{rated}_{BESS}). This MPC design allows the BESSs with high SOC to operate in the discharging mode, and the BESSs with low SOC to operate in the charging mode. In traditional EMS for ES-qZS-CHBMLI, as presented in Section 5 of this paper, all BESSs are kept either in charging or discharging mode simultaneously, without any possibility to operate different BESSs in different modes at the same time. The MPC-EMS design is described below.

The EMS generates the current reference for each BESS ($I^*_{BESS,n}$) according to its state of charge (SOC_n) and the total power of the BESSs ($P_{BESSs,TOT}$). Then, $I^*_{BESS,n}$ is used to obtain P^*_n, as illustrated in Fig. 2. The control scheme of the MPC-EMS is illustrated in Fig. 3. Fig. 3. a represents the control loop for the grid power (P_{grid}). The reference power provided by the system operator must be within the minimum and the maximum available power in the MG ($P_{AV,min}$ and $P_{AV,max}$, respectively). These powers are calculated from the total power of the PV plants ($P_{PV,tot}$) and the minimum and maximum available power in the BESSs (discharge and charge respectively, $P_{BESSs,min}$ and $P_{BESSs,max}$). Therefore, the minimum and maximum available power can be calculated as in (14).

$$P_{AV,min} = P_{PV,tot} - P_{BESSs,min}$$
$$P_{AV,max} = P_{PV,tot} + P_{BESSs,max} \tag{14}$$

The system operator reads $P_{AV,min}$and $P_{AV,max}$ and sets the active power reference (P^*_{grid}) for the MG. It must be noticed that this reference can imply either active power injection or absorption from the main grid, but it must always remain within the maximum and minimum available power in (14). Finally, a PI controller is implemented to define the $P^*_{BESSs,TOT}$ that allows an adequate regulation of the grid active power reference (P^*_{grid}).

The structure of the proposed MPC is shown in Fig. 3.b. MPC is a feedback control technique based on a model and an optimization algorithm for multiple-input multiple-output (MIMO) linear time-invariant (LTI) systems. This controller allows weighting each controlled variable according to its importance in the control of the system. MPC works with three types of variables: manipulated, measured and disturbances. The manipulated variables (MV) are the control signals applied to the plant. The measured outputs (MO) are the signals to be controlled in order to track the imposed references. Additionally, perturbations can be considered through the measured or unmeasured disturbances (MD, UD) inputs. The optimization of the cost function is carried out within a prediction horizon (P_H). The cost function (J) is given by (15):

$$J = \sum_{i=1}^{P_H} [y(k+i|k) - w(k+i|k)]^2 \lambda_1 + \sum_{i=1}^{N} [\Delta u(k+i-1|k)]^2 \lambda_2 \tag{15}$$

This function penalizes the deviation of the measured outputs (y) from their reference values (w) on one hand, and on the other hand, the control effort (Δu) required to track the reference signal. This calculation is carried out each time step (k), for every future instant (i), within a prediction and a control horizon (P_H and N, respectively). Moreover, the relative importance of each term is defined through the weighting matrices λ_1 and λ_2. The aim of MPC is to minimize the cost function (J), that is, to achieve an adequate tracking of the reference signals with the minimum control effort. In this sense, MPC uses quadratic programming (QP) to solve the optimization problem. In this work, the matrices composing the MIMO system for the MPC are:

$$y = \begin{bmatrix} SOC_1 \\ SOC_2 \\ SOC_3 \\ P_{BESSs,TOT} \end{bmatrix} u = \begin{bmatrix} I^*_{BESS,1} \\ I^*_{BESS,2} \\ I^*_{BESS,3} \end{bmatrix}$$

$$w = \begin{bmatrix} SOC^*_1 \\ SOC^*_2 \\ SOC^*_3 \\ P^*_{BESSs,TOT} \end{bmatrix} \lambda_1 = \begin{bmatrix} \tau_1 & 0 & 0 & 0 \\ 0 & \tau_2 & 0 & 0 \\ 0 & 0 & \tau_3 & 0 \\ 0 & 0 & 0 & \tau_4 \end{bmatrix} \lambda_2 = \begin{bmatrix} \gamma_1 & 0 & 0 \\ 0 & \gamma_2 & 0 \\ 0 & 0 & \gamma_3 \end{bmatrix} \tag{16}$$

where $P^*_{BESSs,TOT}$ denotes the reference total power of the BESSs.

As shown in Fig. 3b, the inputs (y) are the SOC and the total power of the BESSs (SOC_n and $P_{BESSs,TOT}$, respectively). The latter is calculated as the sum of the active power of each BESS, as shown in (17)–(18):

$$P_{BESS,n} = V_{BESS,n} \hat{A} \cdot I_{BESS,n} \tag{17}$$

$$P_{BESSs,TOT} = \sum P_{BESS,n} \tag{18}$$

The MPC reference signals (w) are, therefore, the reference SOC (SOC^*_n) and the reference for the total BESSs power ($P^*_{BESSs,tot}$). The outputs (u) of the MPC, i.e. the MVs used to regulate the MOs at their reference values, are the current references for each BESS ($I^*_{BESS,n}$).

The MPC is designed with the *Model Predictive Control Toolbox* from MATLAB/Simulink. The first step in the MPC design is to linearize the plant model with the *Simulink Control Design Toolbox*. To extend the cycle life of the BESS, thresholds are set for their charge and discharge. In this case, the high and low SOC thresholds are set to $SOC_{high} = 90\%$ and $SOC_{low} = 15\%$, respectively. The SOC reference is set to the average

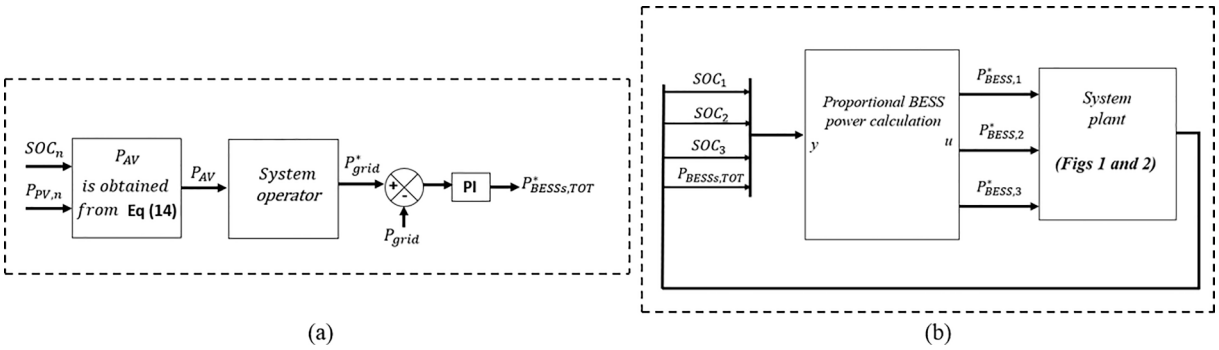

Fig. 4. SOC-EMS overall scheme: (a) Grid power control scheme. (b) Proportional BESS power calculation.

Table 2
BESS parameters.

Symbol	Parameter	Value
V_{BESS}	Rated Voltage (V)	27.5
P_{BESS}^{rated}	Rated Power (W)	1200
Q_{BESS}	Rated Capacity (Ah)	43.63
SOC_1	Initial SOC of BESS 1 (%)	80
SOC_2	Initial SOC of BESS 2 (%)	50
SOC_3	Initial SOC of BESS 3 (%)	20

value between these thresholds, i.e. $SOC_n^* = 52,5\,\%$. The total BESSs power reference ($P^*_{BESSs,TOT}$) is defined using a PI controller that tracks P_{grid} with P^*_{grid}, as illustrated in Fig. 3(a). However, it is necessary to set constraints for the optimization problem. In this case, the BESSs currents and $P_{BESSs,TOT}$ are limited according to their rated values for the charging and discharging modes to $\pm$ 43.63 A and $\pm$ 3600 W, respectively. These are defined as hard constraints, and thus will not be exceeded in the optimization algorithm.

The next step in the design of the MPC is to establish the weighting factors. The MPC prioritizes the tracking of $P^*_{BESSs,TOT}$. Therefore, a weighting factor of 500 is used for $P_{BESSs,TOT}$ (high priority), while a weighting factor of 0.1 (below average priority) is set for SOC_n. An effective monitoring of the BESS power is achieved with these values. This allows optimizing the power absorbed or provided by each BESS according to its SOC. Table 1 summarizes the parameters used in the MPC design.

5. Proportional SOC-Based energy management system (SOC-EMS)

For comparison purposes with the MPC-EMS presented in Section 4, this section describes an alternative EMS with a proportional sharing algorithm based on the SOC of the BESSs (SOC-EMS) [38]. The control scheme implemented for the active and reactive powers is represented in Fig. 4. The grid power control system, represented in Fig. 4.a, is the same as for the MPC-EMS. The BESS power calculation scheme of the SOC-EMS is shown in Fig. 4.b.

The aim of the SOC-EMS is to perform a proportional power distribution among the BESSs according to their SOC. The BESS with the highest SOC is discharged more than the others, and the BESS with the lowest SOC receives more power in the charging mode. The SOC-EMS operates in the charging mode if the total PV power generation is higher than the grid active power reference ($P_{PV\_tot} > P^*_{grid}$). On the other hand, if the total PV power generation is lower than the grid active power reference ($P_{PV\_tot} < P^*_{grid}$), the system operates in the discharging mode. The power of the BESSs for the charging and discharging modes can be calculated according to equations (19) and (20) respectively:

$$P_{BESS,n\_char} = \frac{P_{BESSs,TOT}\,\hat{\mathrm{A}}\cdot DOD_n}{\sum DOD_n} \tag{19}$$

$$P_{BESS,n\_dis} = \frac{P_{BESSs,TOT}\,\hat{\mathrm{A}}\cdot SOC_n}{\sum SOC_n} \tag{20}$$

where P_{BESS,n_char} and P_{BESS,n_dis} are the power for each BESS in the charging and discharging mode, respectively; and DOD_n denotes the depth of discharge for each BESS.

To extend the life of the BESSs, two constraints are implemented. First, the SOC cannot exceed two thresholds, denoted as SOC_{low} for the discharging mode, and SOC_{high} for the charging mode. Second, the maximum power that each BESS can inject or receive is limited to the rated power of the BESSs (P_{BESS}^{rated}). The different operation modes of the SOC-EMS are described as follows:

1. Safe mode ($SOC_{low} < SOC_n < SOC_{high}$): All BESSs operate in the discharging or charging mode at the same time according to Eqs. (20) and (21).
2. High SOC mode ($SOC_n \geq SOC_{high}$): If the SOC of a certain BESS exceeds the maximum limit, and the BESSs are operating in the charging mode, that specific BESS cannot be charged higher. The SOC-EMS sets the power of that BESS to zero and the remaining BESSs continue operating in the charging mode until they reach SOC_{high}.
3. Low SOC mode ($SOC_n \leq SOC_{low}$): If the SOC of a certain BESS is below the minimum limit, and the BESSs are operating in the discharging mode, that specific BESS cannot be discharged deeper. The SOC-EMS sets the power of that BESS to zero and the remaining BESSs continue operating in the discharging mode until they reach SOC_{low}.

6. Results and discussion

This section evaluates the effectiveness of the proposed control system and the MPC-EMS under variable solar irradiation, and active and reactive power references defined by the system operator. The proposed MPC-EMS is compared with the proportional sharing algorithm based on the SOC of the BESSs described in Section 5 (denoted as SOC-EMS) to demonstrate the improved control and optimal sharing of the BESSs powers achieved with the MPC-ESS. The simulation is implemented in MATLAB/Simulink. Finally, to validate the proposed MPC-EMS with experimental results, a Hardware-in-the-Loop experimental setup has been implemented in the laboratory with an OPAL RT-4015 unit, to execute the system under study in real-time, and a dSPACE MicroLabBox prototyping unit to implement the control systems. A Yokogawa DLM4038 oscilloscope measures and represents the variables of interest in real time, and registers the experimental results shown in this section.

Table 3
Impedance network parameters.

Symbol	Parameter	Value
$L_1 = L_2$	Inductance (mH)	0.56
$R_1 = R_2$	Resistance (Ω)	0.05
$C_1 = C_2$	Capacitance (mF)	11

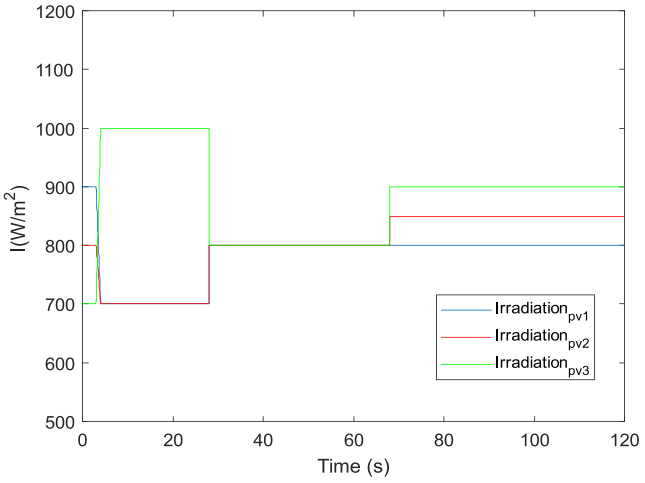

Fig. 5. Irradiation of PV1, PV2 and PV3.

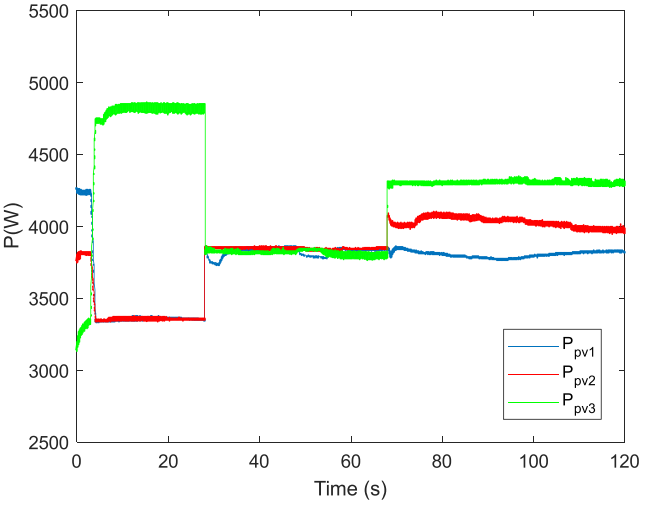

Fig. 6. Power generated by PV1, PV2 and PV3.

6.1. Case study

The ES-qZS-CHBMLI comprises three independent 4.8 kW PV generators. Each PV system consists of 6 strings of 2 modules in series, with a rated power of 400 W for each module. The main parameters of the BESS connected in parallel with the capacitor $C_{2,n}$ are summarized in Table 2, and the values of the impedance network for each module are given in Table 3.

6.2. Simulation results

A 120 s simulation is performed in MATLAB/Simulink. The sample time selected for this simulation is $T_s = 10\,\mu s$ and the carrier frequency for the inverter modulation technique is set to $f_c = 3.5\,kHz$. The base power of the power system is set to $P_B = 4.8\,kW$. The temperature of all the PV modules is set to 25 °C, and it remains constant for the whole simulation.

Fig. 5 depicts the irradiation of the three modules. PV power plant 1 (PV1) starts at 900 W/m^2, then changes to 700 W/m^2 at 3 s and finally to 800 W/m^2 at 30 s. PV power plant 2 (PV2) starts at 800 W/m^2, the irradiation varies to 700 W/m^2 at 3 s, to 800 W/m^2 at 30 s, and increases to 850 W/m^2 at 70 s. Finally, PV power plant 3 (PV3) starts at 700 W/m^2, then changes to 1000 W/m^2 at 3 s, to 800 W/m^2 at 30 s, and to 900 W/m^2 at 70 s. Fig. 6 shows the output power of each PV plant. It can be seen that the power variations coincide with the variations in the irradiation. PV3 generates at its rated power between 3 and 30 s because the

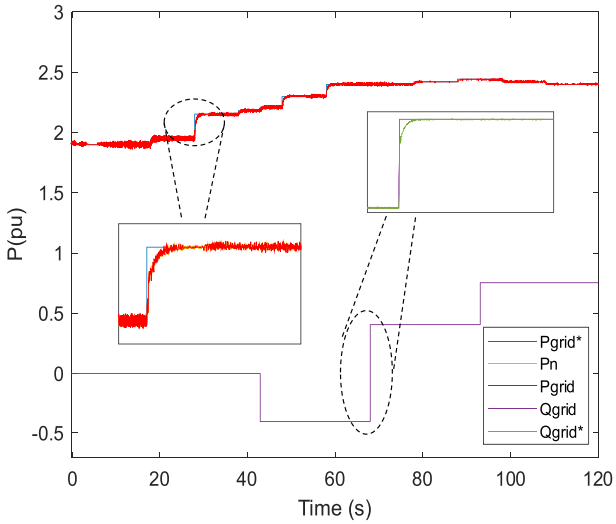

Fig. 7. Grid active (P_{grid}) and reactive power (Q_{grid}), and the sum of the active power of each module at the VSI input (P_n).

Table 4
Grid active and reactive power references profile.

Time (s)	P^*_{grid} (pu)
[0 20]	1.9
[20 30]	1.95
[30 40]	2.15
[40 45]	2.18
[45 50]	2.21
[50 60]	2.3
[60 65]	2.4
[65 70]	2.4
[70 80]	2.4
[80 90]	2.42
[90 100]	2.44
[100 110]	2.42
[110 120]	2.4
	Q^*_{grid} (pu)
[0 45]	0
[45 70]	−0.4
[70 95]	0.4
[95 120]	0.75

Table 5
ITAE for MPC-EMS and SOC-EMS.

Parameter	Value
$ITAE\_P_{grid}$(SOC-EMS)	33.95
$ITAE\_P_{grid}$(MPC-EMS)	27.26 (−20 %)
$ITAE\_Q_{grid}$(SOC-EMS)	14.37
$ITAE\_Q_{grid}$(MPC-EMS)	13.79 (−4 %)

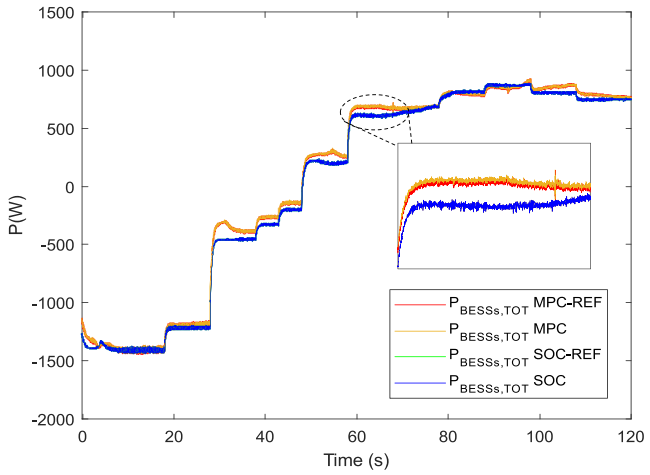

Fig. 8. Total BESSs power for MPC-EMS and SOC-EMS.

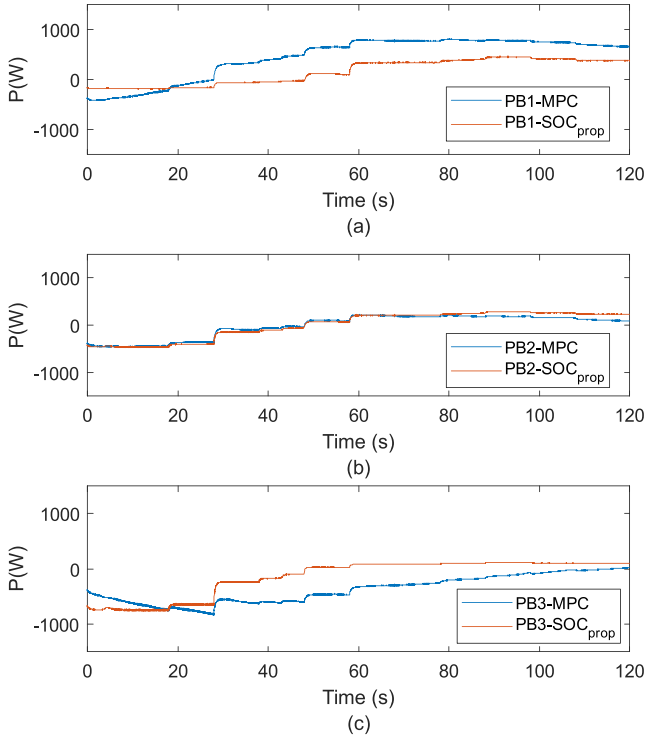

Fig. 9. BESS power: (a) PB1, (b) PB2, (c) PB3.

irradiation received is 1000 W/m^2.

Fig. 7 depicts the active and reactive power delivered to the grid, as well as the sum of the active power of each module at the VSI input. The system is tested under variable power references, as shown in Table 4. From 0 to 50 s, the BESSs operate in the charging mode because $P_{PV} > P^*_{grid}$. When P^*_{grid} increases, the BESSs consequently decrease their charging power. At 50 s, $P_{PV} = P^*_{grid}$, and the BESSs are neither charged nor discharged. From 50 to 120 s, the BESSs operate in the discharging mode because $P_{PV} < P^*_{grid}$. As P^*_{grid} increases, the BESSs have to provide more power to satisfy the demand of the system operator. The reactive power exchanged with the grid is also tested under three different situations. From 0 to 45 s, the grid reactive power reference (Q^*_{grid}) is set to 0 to achieve unity power factor. From 45 to 70 s, the system operator sets $Q^*_{grid} = 1920\ VAR$ capacitive. Finally, reactive power is injected to the grid from 70 to 95 s, being $Q^*_{grid} = 1920\ VAR$ inductive, and increasing to $Q^*_{grid} = 3600\ VAR$ inductive from 95 to 120 s. The results show that the configuration and the control system implemented respond to these changes effectively.

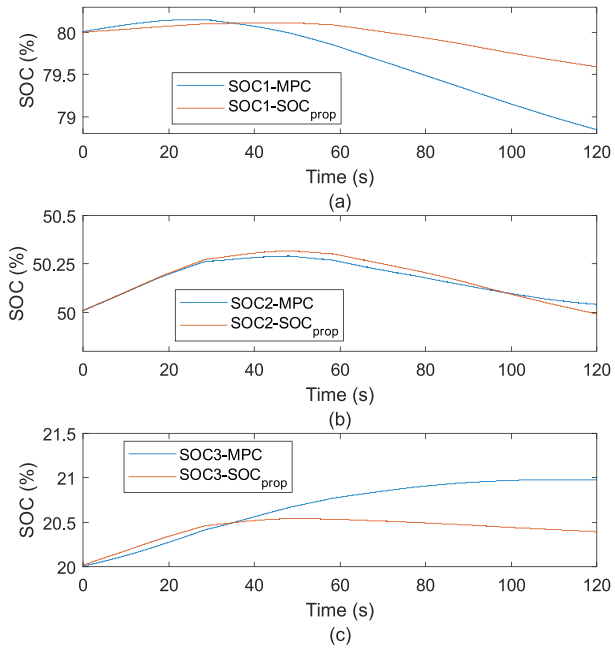

Fig. 10. SOC levels: (a) BESS 1, (b) BESS 2, (c) BESS 3.

Table 6
SOC values for MPC-EMS and SOC-EMS.

Parameter	Value
SOC_1(MPC-EMS)	78.85 %
SOC_1(SOC-EMS)	79.57 %
SOC_2(MPC-EMS)	50.04 %
SOC_2(SOC-EMS)	49.98 %
SOC_3(MPC-EMS)	20.98 %
SOC_3(SOC-EMS)	20.39 %

In order to evaluate the performance of the controllers quantitatively, the integral time absolute error (ITAE) is calculated for P_{grid} and Q_{grid}:

$$ITAE = \int |e| \hat{A} \cdot dt \tag{21}$$

where $|e|$ denotes the module of the error between P^*_{grid} and P_{grid} (for $ITAE\_P_{grid}$) or between Q^*_{grid} and Q_{grid} (for $ITAE\_Q_{grid}$).

The ITAE obtained with the proposed MPC-EMS and with the benchmark SOC-EMS for the 120 s simulation are listed in Table 5.

These results illustrate that the MPC-EMS achieves a better control of P_{grid} and Q_{grid} than the SOC-EMS, with a 20 % reduction on $ITAE\_P_{grid}$, and a 4 % reduction on $ITAE\_Q_{grid}$ for the former.

Fig. 8 presents the total BESSs power for both EMS. Firstly, it can be highlighted that the MPC-EMS tracks the changes in $P^*_{BESSs,TOT}$ effectively, which is one of its main objectives. In addition, the $P_{BESSs,TOT}$ obtained with the SOC-EMS differs from that obtained with MPC-EMS. This is because the tracking error of P_{grid} is lower for the MPC-EMS, as previously shown in Table 5. Subsequently, the output of the PI controller ($P_{BESSs,TOT}$) differs for both EMS. The aim of the MPC-EMS is to achieve an optimal BESS power sharing. This implies that it prioritizes charging the BESS with the lowest SOC, while discharging the BESS with the highest SOC simultaneously. In contrast, the SOC-EMS performs a

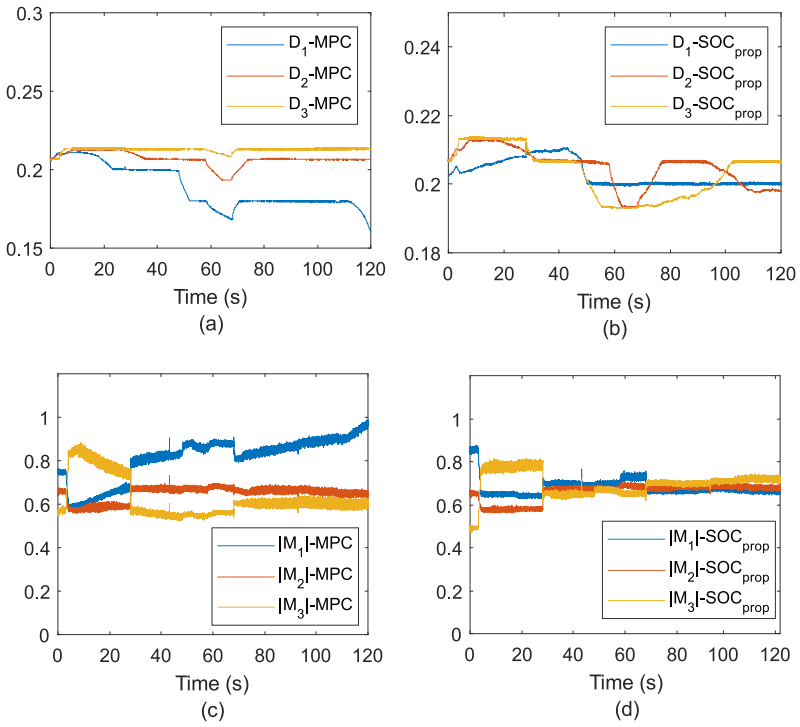

Fig. 11. Shoot-through duty ratio (D) and modulation index (M) for the three inverters in series: (a) D for qZSI-1 (D1), qZSI2 (D2) and qZSI3 (D3) with the MPC-EMS. (b) D for qZSI-1 (D1), qZSI-2 (D2) and qZSI-3 (D3) with the SOC-EMS. (c) M for qZSI-1 (M1), qZSI-2 (M2) and qZSI-3 (M3) with the MPC-EMS. (d) M for qZSI-1 (M1), qZSI-2 (M2) and qZSI-3 (M3) with the SOC-EMS.

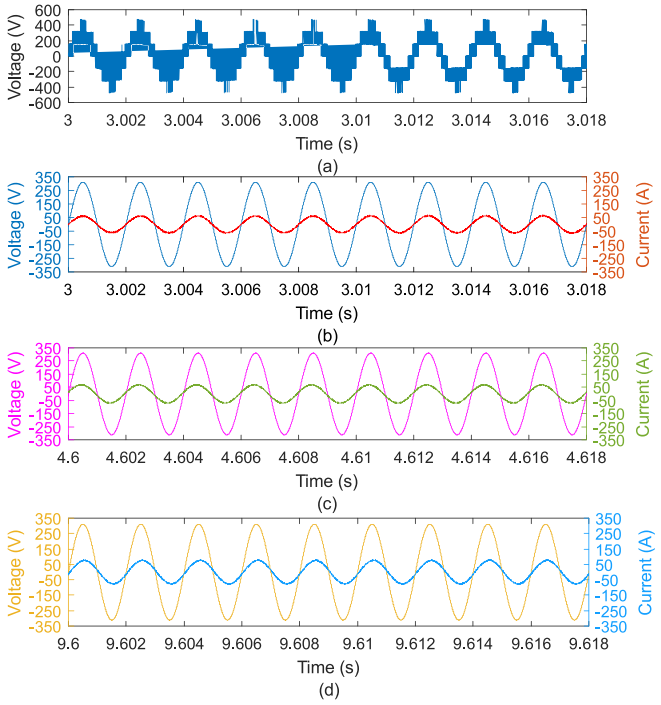

Fig. 12. Grid measurements: (a) Seven-level output voltage of ES-qZS-CHBMLI. (b) Grid voltage and current with unity power factor. (c) Grid voltage and current with 0.984 capacitive power factor. (d) Grid voltage and current with 0.954 inductive power factor.

power sharing where all the BESSs are charged (discharged) when the total BESS power sets the charge (discharge) mode. Therefore, the MPC-EMS allows charging and discharging processes at the same time for different BESSs, providing a more efficient distribution of the total BESS power.

Fig. 9(a)-(c) illustrate the power of each BESS for both EMSs. It can be seen in Fig. 9(a) that, for the MPC-EMS, the BESS 1 (PB1) starts discharging at 30 s, whereas for the SOC-EMS, it starts at 50 s. On the other hand, the BESS 3 (PB3) always operates in charging mode for the MPC-EMS (Fig. 9(c)), whereas for the SOC-EMS, it operates in the charging mode from 0 to 50 s, and in discharging mode from 50 to 120 s. This demonstrates that the MPC-EMS prioritizes charging the BESS with lowest SOC, as discussed above.

The evolution of the SOC throughout the simulation is represented in Fig. 10. Fig. 10(a)-(c) show the SOC levels at the end of simulation for both EMS. These values are summarised in Table 6. The results show that, with the MPC-EMS, the BESS 1 is discharged deeper and BESS 3 is charged higher than with the SOC-EMS.

The values of D and M for the three inverters of the cascaded H-bridge multilevel inverter are shown in Fig. 11. As seen, the inverters controlled with the MPC-EMS present less variability in the control of D (Fig. 11a) in comparison with the SOC-EMS (Fig. 11b). Subsequently, better results are achieved with the MPC-EMS for the MPPT in the PV systems, owing to the control of D. On the other hand, there are significant differences between M1 and M3 in the MPC-EMS (Fig. 11c); whereas M1, M2 and M3 achieved with the SOC-EMS are similar (Fig. 11d). These differences in M support the differences between the powers of BESS1 and BESS3 observed in Fig. 9.

Fig. 12(a) depicts the seven-level output voltage of the ES-qZS-CHBMLI. Fig. 12(b) shows the grid voltage and current with unity power factor. Fig. 12(c) illustrates the grid voltage and current with capacitive power factor of 0.984 (P_{grid} = 10680 W, Q_{grid} = 1920 VAR). Finally, Fig. 12(d) represents the grid voltage and current with inductive power factor of 0.954 (P_{grid} = 11520 W, Q_{grid} = 3629 VAR).

6.3. Experimental results

The Hardware-in-the-Loop (HIL) experimental setup implemented in

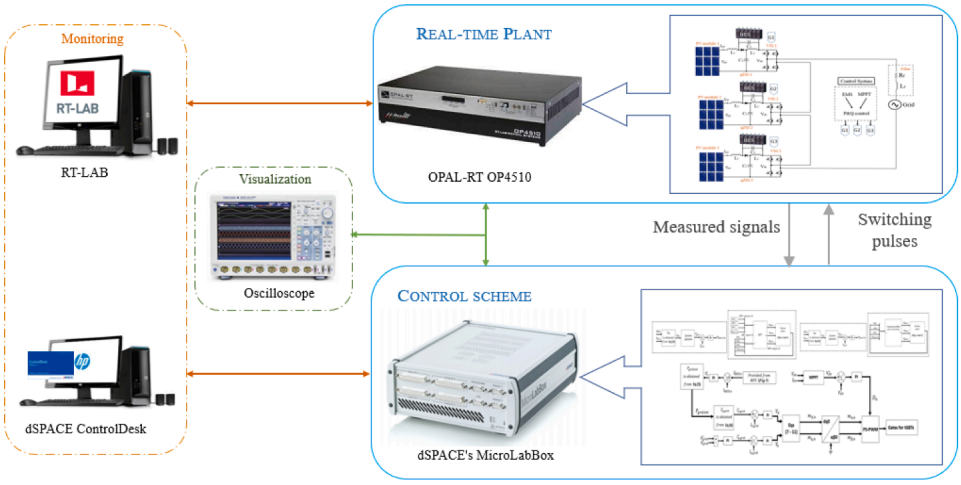

(a)

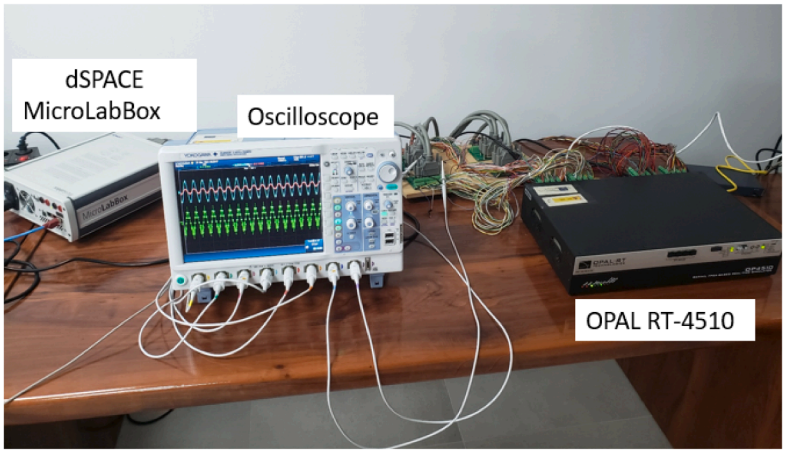

(b)

Fig. 13. HIL experimental setup implemented in the laboratory: (a) Scheme. (b) Photo.

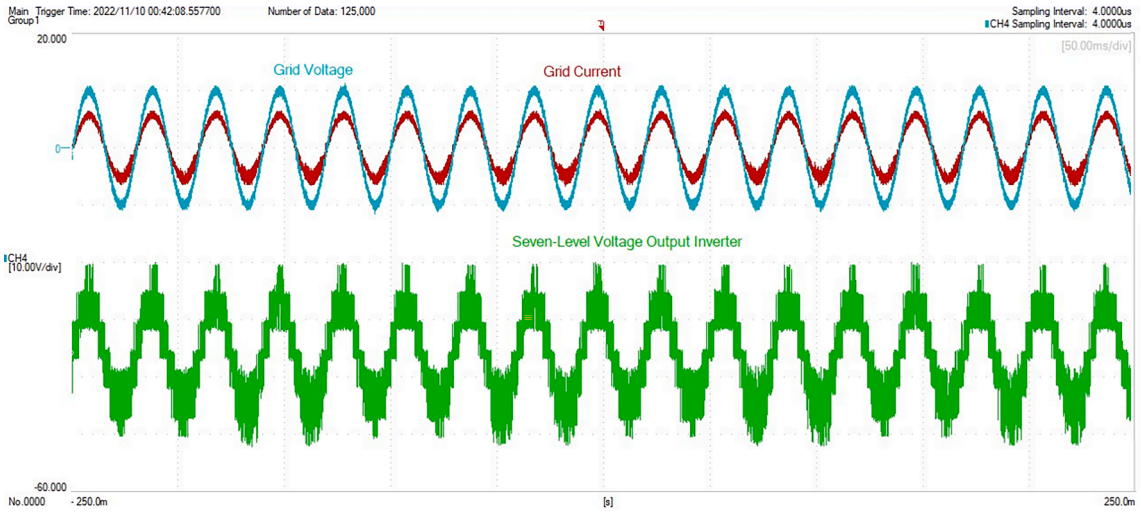

Fig. 14. Experimental results for grid voltage, grid current, and seven-level voltage output inverter with unity power factor.

the laboratory to validate the solutions proposed in this work is shown in Fig. 13. The OPAL RT-4510 unit runs the MG model under study in real time. The RT-Lab software is used to program and monitor the model in real time. The control system and the proposed EMS are implemented in a dSPACE MicroLabBox prototyping unit. The dSPACE ControlDesk software allows monitoring, evaluating, and controlling the execution of the control system in real time. Finally, to measure and represent the inputs and outputs of both devices, a Yokogawa DLM4038 oscilloscope

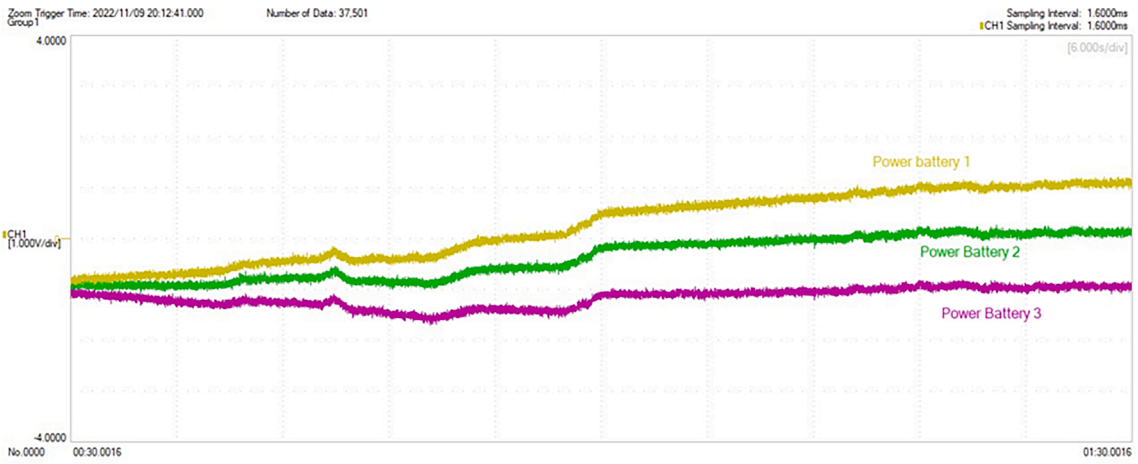

Fig. 15. Experimental results for the BESS power (PB1, PB2, and PB3) with MPC-EMS.

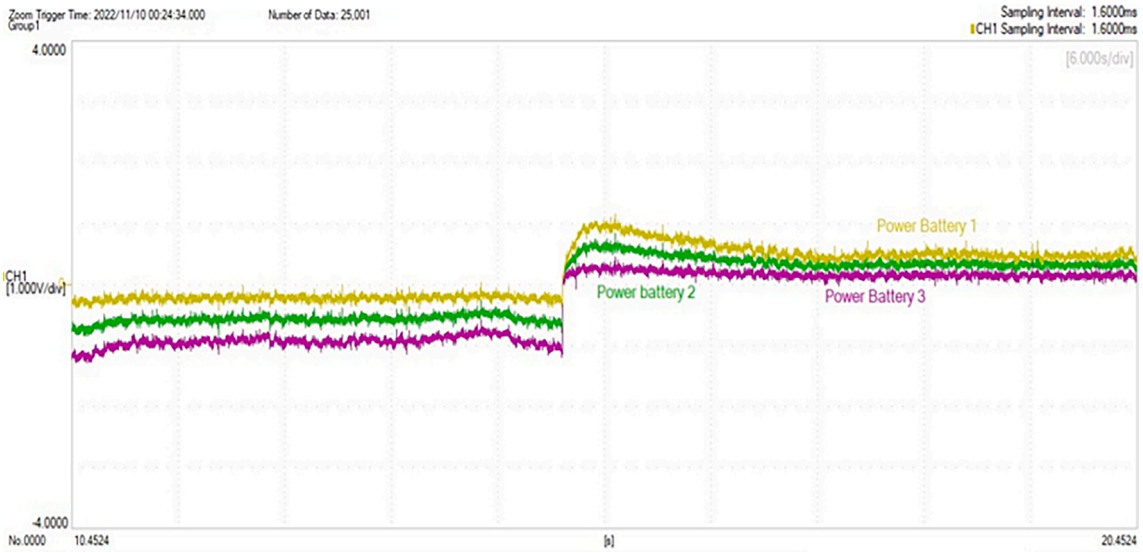

Fig. 16. Experimental results for the BESS power (PB1, PB2, and PB3) with SOC-EMS.

is used. A similar HIL experimental setup was used in [39,40]. An OPAL5600 simulator was used in [39] to run the power plant in real time, and three DSP controllers were used to implement the EMS. In [40], the system under study was implemented in a Typhoon HIL-402 device, and the EMS was developed in MATLAB.

Fig. 14 shows the experimental results of the seven-level output voltage of the ES-qZS-CHBMLI. In this figure, the grid voltage and current are in phase, because the system is operating with unity power factor. These results are consistent with the simulation results shown in Fig. 12(a) and (b), respectively. The power of each BESS (PB1, PB2, and PB3) obtained with the MPC-EMS are illustrated in Fig. 15. During the charging mode, the BESS 3 is charged higher than BESS 2 and BESS 1. Similarly, during the discharging mode, BESS 3 is charged owing to its low SOC, although the other BESSs are discharged. Fig. 16 shows the power of each BESS (PB1, PB2, and PB3) for SOC-EMS. The experimental results are again consistent with the simulation results. In this sense, the MPC-EMS charges the BESS 3 more than the SOC-EMS, whereas the BESS 1 is discharged deeper with the MPC-EMS than with the SOC-EMS.

7. Conclusions

This work presented an optimal EMS based on MPC for a MG with PV generation, BESS and a qZSI-CHBMLI. This MPC-EMS enables a more efficient power sharing among the BESSs considering their SOC and the total BESSs power exchange, and thus, an optimal operation of the BESSs smoothing variations in the PV power generation. The system was evaluated under different irradiation and changes in the grid operator active and reactive power demand. The simulation results showed a satisfactory control of the power delivered to the grid, and the power distribution among the BESSs. In addition, the experimental results obtained with OPAL RT-4510 and dSPACE MicroLabBox were consistent with the simulation results. The MPC-EMS was compared with an EMS that used a proportional sharing algorithm based on the SOC of the BESS (SOC-EMS). The results showed that the MPC-EMS improved the control of the active power delivered to the grid (20 % reduction on ITAE) and the reactive power (4 % reduction on ITAE) compared to the SOC-EMS. The SOCs achieved with the MPC-EMS were higher than those achieved with the SOC-EMS, because charging the BESS with lower SOC was prioritized.

This work presented an MPC-EMS for a MG under normal operation. Future studies could include a control scheme for scenarios in which faults occur in PV power plants or H-bridges. Furthermore, new objective functions could be added to the control scheme to improve the efficiency of the MG operation. New RETs and ESSs, such as wind turbines, ultracapacitors or green hydrogen systems (fuel cells and electrolyzers) could be added to evaluate the effectiveness of the proposed MPC-EMS

under hybrid configurations combining several types of RETs and ESSs.

CRediT authorship contribution statement

Pablo Horrillo-Quintero: Conceptualization, Formal analysis, Investigation, Methodology, Writing – original draft. **Pablo García-Triviño:** Conceptualization, Formal analysis, Investigation, Methodology, Writing – original draft. **Raúl Sarrias-Mena:** Conceptualization, Formal analysis, Investigation, Methodology, Writing – original draft. **Carlos A. García-Vázquez:** Formal analysis, Methodology, Writing – original draft. **Luis M. Fernández-Ramírez:** Conceptualization, Funding acquisition, Methodology, Project administration, Supervision, Writing – review & editing.

Declaration of Competing Interest

The authors declare that they have no known competing financial interests or personal relationships that could have appeared to influence the work reported in this paper.

Data availability

The authors are unable or have chosen not to specify which data has been used.

Acknowledgments

This work is partially supported by the Regional Ministry of Economic Transformation, Industry, Knowledge, and Universities of Junta de Andalucía (under Grant PY20_00317), and Ministerio de Ciencia e Innovación, Agencia Estatal de Investigación, FEDER, UE (Grant PID2021-123633OB-C32 supported by MCIN/AEI/10.13039/501100011033/ FEDER, UE).

References

[1] "A Clean Planet for All: Europe's long-term strategic vision for a prosperous, modern, competitive and climate-neutral economy" [Online]. Available: https://eur-lex.europa.eu/legalcontent/ES/TXT/?uri=CELEX%3A52018DC0773.
[2] Shahbazitabar M, Abdi H, Nourianfar H, Anvari-Moghaddam A, Mohammadi-Ivatloo B, Hatziargyriou N. An Introduction to Microgrids, Concepts, Definition, and Classifications. In: Anvari-Moghaddam A, Abdi H, Mohammadi-Ivatloo B, Hatziargyriou N, editors. Microgrids: Advances in Operation, Control, and Protection. Cham: Springer International Publishing; 2021. p. 3–16. https://doi.org/10.1007/978-3-030-59750-4_1.
[3] Vasilakis A, Zafeiratou I, Lagos DT, Hatziargyriou ND. The Evolution of Research in Microgrids Control. IEEE Open Access J Power Energy 2020;7:331–43. https://doi.org/10.1109/OAJPE.2020.3030348.
[4] "2012 DOE Microgrid Workshop Report." [Online]. Available: http://energy.gov/sites/prod/files/Microgrid%20Workshop%20Report%20August%202011.pdf.
[5] I. Renewable Energy Agency, Global Energy Transformation: A Roadmap to 2050. 2018. [Online]. Available: www.irena.org.
[6] Cabrera-Tobar A, Bullich-Massagué E, Aragüés-Peñalba M, Gomis-Bellmunt O. Topologies for large scale photovoltaic power plants. Renew Sustain Energy Rev 2016;59:309–19. https://doi.org/10.1016/j.rser.2015.12.362.
[7] de Oliveira-Assis L, Soares-Ramos EPP, Sarrias-Mena R, García-Triviño P, González-Rivera E, Sánchez-Sainz H, et al. Simplified model of battery energy-stored quasi-Z-source inverter-based photovoltaic power plant with Twofold energy management system. Energy 2022:244. https://doi.org/10.1016/j.energy.2021.122563.
[8] Vavilapalli S, Umashankar S, Sanjeevikumar P, Ramachandaramurthy VK, Mihet-Popa L, Fedák V. Three-stage control architecture for cascaded H-Bridge inverters in large-scale PV systems – Real time simulation validation. Appl Energy 2018;229:1111–27. https://doi.org/10.1016/j.apenergy.2018.08.059.
[9] Sanchis P, Gubia E, Marroyo L. Cascaded H-Bridge Multilevel Converter for Grid Connected Photovoltaic Generators with Independent Maximum Power Point Tracking of each Solar Array. n.d.
[10] Sun D, Ge B, Yan X, Bi D, Zhang H, Liu Y, et al. Modeling, impedance design, and efficiency analysis of quasi-Z source module in cascaded multilevel photovoltaic power system. IEEE Trans Ind Electron 2014;61:6108–17. https://doi.org/10.1109/TIE.2014.2304913.
[11] Balamurugan CR, Vijayalakshmi K. Comparative analysis of various Z-source based five level cascaded H-bridge multilevel inverter. Bull Elect Eng Inform 2018;7:1–14. 10.11591/eei.v7i1.656.
[12] Liang W, Liu Y, Peng J. A Day and Night Operational Quasi-Z Source Multilevel Grid-Tied PV Power System to Achieve Active and Reactive Power Control. IEEE Trans Power Electron 2021;36:474–92. https://doi.org/10.1109/TPEL.2020.3000818.
[13] Li K, Tseng KJ. Energy efficiency of lithium-ion battery used as energy storage devices in micro-grid. In: IECON 2015–41st Annual Conference of the IEEE Industrial Electronics Society. Institute of Electrical and Electronics Engineers Inc.; 2015. p. 5235–40. https://doi.org/10.1109/IECON.2015.7392923.
[14] Sun D, Ge B, Liang W, Abu-Rub H, Peng FZ. An energy stored Quasi-Z-Source cascade multilevel inverter-based photovoltaic power generation system. IEEE Trans Ind Electron 2015;62:5458–67. https://doi.org/10.1109/TIE.2015.2407853.
[15] Ge B, Liu Y, Abu-Rub H, Peng FZ. State-of-Charge Balancing Control for a Battery-Energy-Stored Quasi-Z-Source Cascaded-Multilevel-Inverter-Based Photovoltaic Power System. IEEE Trans Ind Electron 2018;65:2268–79. https://doi.org/10.1109/TIE.2017.2745406.
[16] Huang W, Abu Qahouq JA. Energy Sharing Control Scheme for State-of-Charge Balancing of Distributed Battery Energy Storage System. IEEE Trans Ind Electron 2015;62:2764–76. https://doi.org/10.1109/TIE.2014.2363817.
[17] Lu X, Sun K, Guerrero JM, Vasquez JC, Huang L. State-of-charge balance using adaptive droop control for distributed energy storage systems in DC microgrid applications. IEEE Trans Ind Electron 2014;61:2804–15. https://doi.org/10.1109/TIE.2013.2279374.
[18] Byrne RH, Nguyen TA, Copp DA, Chalamala BR, Gyuk I. Energy Management and Optimization Methods for Grid Energy Storage Systems. IEEE Access 2017;6:13231–60. https://doi.org/10.1109/ACCESS.2017.2741578.
[19] Suganthi L, Iniyan S, Samuel AA. Applications of fuzzy logic in renewable energy systems - A review. Renew Sustain Energy Rev 2015;48:585–607. https://doi.org/10.1016/j.rser.2015.04.037.
[20] García-Triviño P, Sarrias-Mena R, García-Vázquez CA, Leva S, Fernández-Ramírez LM. Optimal online battery power control of grid-connected energy-stored quasi-impedance source inverter with PV system. Appl Energy 2023;329:120286. https://doi.org/10.1016/j.apenergy.2022.120286.
[21] Li L, Yang T, Yuan Y, Cai Z. A model predictive control strategy based on energy storage grid-connected quasi-z-source inverters. IET Gener Transm Distrib 2022;16:3451–61. https://doi.org/10.1049/gtd2.12534.
[22] Kumar K, Bae S. Dynamic power management based on model predictive control for hybrid-energy-storage-based grid-connected microgrids. Int J Electr Power Energy Syst 2022:143. https://doi.org/10.1016/j.ijepes.2022.108384.
[23] Petrollese M, Valverde L, Cocco D, Cau G, Guerra J. Real-time integration of optimal generation scheduling with MPC for the energy management of a renewable hydrogen-based microgrid. Appl Energy 2016;166:96–106. https://doi.org/10.1016/j.apenergy.2016.01.014.
[24] Valverde L, Bordons C, Rosa F. Integration of fuel cell technologies in renewable-energy-based microgrids optimizing operational costs and durability. IEEE Trans Ind Electron 2016;63:167–77. https://doi.org/10.1109/TIE.2015.2465355.
[25] Batiyah S, Sharma R, Abdelwahed S, Alhosaini W, Aldosari O. Predictive Control of PV/Battery System under Load and Environmental Uncertainty. Energies (Basel) 2022:15. https://doi.org/10.3390/en15114100.
[26] Hu J, Xu Y, Cheng KW, Guerrero JM. A model predictive control strategy of PV-Battery microgrid under variable power generations and load conditions. Appl Energy 2018;221:195–203. https://doi.org/10.1016/j.apenergy.2018.03.085.
[27] Shan Y, Hu J, Chan KW, Fu Q, Guerrero JM. Model Predictive Control of Bidirectional DC-DC Converters and AC/DC Interlinking Converters-A New Control Method for PV-Wind-Battery Microgrids. IEEE Trans Sustain Energy 2019;10:1823–33. https://doi.org/10.1109/TSTE.2018.2873390.
[28] Kou P, Liang D, Wang J, Gao L. Stable and Optimal Load Sharing of Multiple PMSGs in an Islanded DC Microgrid. IEEE Trans Energy Convers 2018;33:260–71. https://doi.org/10.1109/TEC.2017.2755461.
[29] Dragicevic T. Model Predictive Control of Power Converters for Robust and Fast Operation of AC Microgrids. IEEE Trans Power Electron 2018;33:6304–17. https://doi.org/10.1109/TPEL.2017.2744986.
[30] Garcia-Torres F, Valverde L, Bordons C. Optimal Load Sharing of Hydrogen-Based Microgrids with Hybrid Storage Using Model-Predictive Control. IEEE Trans Ind Electron 2016;63:4919–28. https://doi.org/10.1109/TIE.2016.2547870.
[31] Karami Z, Shafiee Q, Khayat Y, Yaribeygi M, Dragicevic T, Bevrani H. Decentralized Model Predictive Control of DC Microgrids with Constant Power Load. IEEE J Emerg Sel Top Power Electron 2021;9:451–60. https://doi.org/10.1109/JESTPE.2019.2957231.
[32] Jayachandran M, Ravi G. Predictive power management strategy for PV/battery hybrid unit based islanded AC microgrid. Int J Electr Power Energy Syst 2019;110:487–96. https://doi.org/10.1016/j.ijepes.2019.03.033.
[33] Jayachandran M, Ravi G. Decentralized model predictive hierarchical control strategy for islanded AC microgrids. Electr Pow Syst Res 2019;170:92–100. https://doi.org/10.1016/j.epsr.2019.01.010.
[34] Jain S, Shadmand MB, Balog RS. Decoupled active and reactive power predictive control for PV applications using a grid-tied quasi-Z-Source inverter. IEEE J Emerg Sel Top Power Electron 2018;6:1769–82. https://doi.org/10.1109/JESTPE.2018.2823904.
[35] Liu Y, Abu-Rub H, Ge B, Blaabjerg F, Ellaban O, Chiang P. Impedance Source Power Electronic Converters. Chichester, UK: John Wiley and Sons-IEEE Press; 2016.
[36] Sun D, Ge B, Peng FZ, Haitham AR, Bi D, Liu Y. A new grid-connected PV system based on cascaded H-bridge quasi-Z source inverter. In: IEEE International Symposium on Industrial Electronics, 2012, p. 951–6. https://doi.org/10.1109/ISIE.2012.6237218.
[37] Maiti S, Sonar S, Ashraf S. Analysis and Comparison of Impedance Source Inverter with different suitable PWM approaches. In: Proceedings - 2022 6th International

Conference on Intelligent Computing and Control Systems, ICICCS 2022. Institute of Electrical and Electronics Engineers Inc.; 2022. p. 321–6. https://doi.org/10.1109/ICICCS53718.2022.9788211.

[38] Horrillo-Quintero P, García-Triviño P, Sarrias-Mena R, García-Vázquez CA, Fernández Ramírez LM, "Control System for Quasi-Z-Source Cascaded H-bridge Multilevel Inverter with PV Power Generation and battery Energy Storage System" Interdisciplinary Conference on Mechanics, Computers and Electrics (ICMECE 2022) 6-7 October 2022, Barcelona, Spain.

[39] Li X, Dong C, Jian W, Wu X. An improved coordination control for a novel hybrid AC/DC microgrid architecture with combined energy storage system. Appl Energy 2021;292. https//doi.org/10.1016/j.apenergy.2022.116824.

[40] Rodriguez M, Arcos-Aviles D, Martinez W. Fuzzy logic-based energy management for isolated microgrid using meta-heuristic optimization algorithms. Appl Energy 2023;335 https://doi.org/j.apenergy.2023.120771.